Density Peaking, Anomalous Pinch, and Collisionality in Tokamak Plasmas

C. Angioni, A. G. Peeters, G. V. Pereverzev, F. Ryter, G. Tardini, and ASDEX Upgrade Team
Max-Planck-Institut für Plasmaphysik, IPP-EURATOM Association, D-85748 Garching bei München, Germany
(Received 9 January 2003; published 22 May 2003)

The existence of an anomalous particle pinch in magnetized tokamak plasmas is still questioned. Contradictory observations have been collected so far in tokamaks. Clear experimental evidence that density peaking in tokamak plasmas drops with increasing collisionality is provided for the first time. This phenomenon is explained by means of existing theoretical models based on the fluid description of drift wave instabilities, provided that such models include the dissipative effects introduced by collisions on the mentioned instabilities. These results reconcile the apparent contradictions found so far in the experiments.

DOI: 10.1103/PhysRevLett.90.205003 PACS numbers: 52.25.Fi, 52.35.Kt, 52.55.Fa

Measured density profiles in tokamaks are usually not completely flat, although the particle source is in general only peripheral. Neoclassical theory predicts the existence of a particle pinch proportional to the inductive electric field of the tokamak, the Ware pinch [1]. However, in several tokamak experiments an anomalous pinch contribution on top of the neoclassical pinch is necessary to explain the observed density peaking [2–6]. In contradiction, other experimental observations, even in the same tokamak, suggest that a pinch of the order of the neoclassical pinch is sufficient to explain the experimental measurements, in plasmas at high density [7,8]. In the present Letter we show that such a contradiction is only apparent and that different observations are consistent with the predictions of a theoretical model based on the fluid description of drift wave instabilities, provided that such model includes the dissipative effects introduced by collisions on the mentioned instabilities. Drift wave instabilities, and, in particular, ion temperature gradient (ITG) and trapped electron modes (TEM), have been found to predict an anomalous heat transport in agreement with the experiment (e.g., [9]); however, particle transport has been poorly explored so far.

Here we give the first clear experimental evidence that collisionality plays a relevant role in determining the density peaking in tokamak plasmas. In Fig. 1, the density peaking of plasmas in stationary conditions and in high confinement mode (H mode), produced in the ASDEX Upgrade tokamak with neutral beam injection (NBI) heating, is plotted versus a dimensionless collisional frequency $\nu_{\rm eff}$, defined as the ratio of the electron-ion collision frequency to the curvature drift frequency. The latter $\omega_{De} = 2k_\perp \rho_s c_s/R$ provides an estimate of the growth rate of the most unstable mode for drift wave instabilities. Here $k_\perp$ is the wave number in the direction perpendicular to the magnetic field line and is estimated $k_\perp \rho_s = \sqrt{0.1}$, $\rho_s = c_s/\Omega_{ci}$, $c_s = \sqrt{T_e/m_i}$, $\Omega_{ci} = Z_i eB/m_i$, and R is the tokamak major radius. Plasmas considered in Fig. 1(a) are all heated with 5 MW of NBI power. Different values of the edge safety factor are plotted with different symbols. The safety factor profile has already been found to play a major role in determining the density profile [2,4]. Figure 1(a) shows that density peaking is also a function of collisionality and, in particular, that it decreases strongly with increasing collisionality for $\nu_{\rm eff} \leq 1$. This behavior is found again in Fig. 1(b) where we have plotted plasmas of two density windows ($0.5 < n_{el20} < 0.55$ and $0.75 < n_{el20} < 0.8$, where n_{el20} is the line average density in dimensions 10^{20} m^{-3}), and edge safety factor $q_{95} \simeq 4$. A wide range

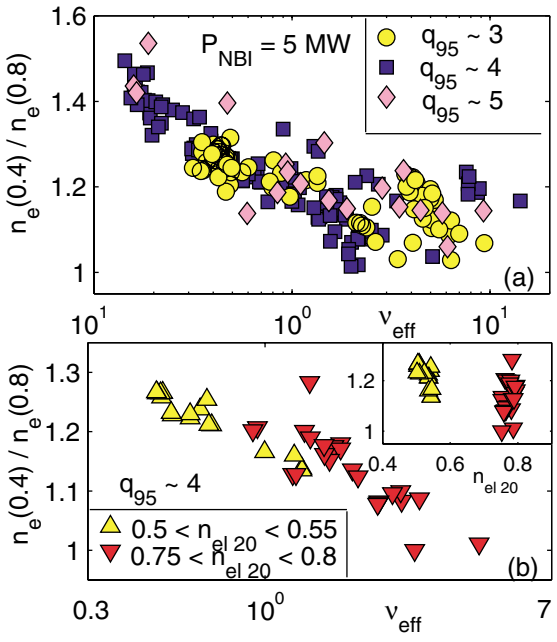

FIG. 1 (color online). Density peaking, $n_e(\rho_\Psi = 0.4)/n_e(\rho_\Psi = 0.8)$ versus $\nu_{\rm eff}$, for two subsets of stationary plasmas in AUG H modes, with NBI heating ($\rho_\Psi \doteq \sqrt{\Psi/\Psi_{\rm edge}}$, where Ψ is the poloidal magnetic flux). (a) Plasmas with 5 MW of NBI power; (b) plasmas with $q_{95} \simeq 4$ in two density windows, $0.5 < n_{el20} < 0.55$ and $0.75 < n_{el20} < 0.8$ (density peaking versus line average density is plotted in the little panel on the right).

of variation of peaking is covered by the selected data points for fixed values of the plasma density, due to variations of the electron temperature. The density peaking shows a much stronger correlation with $\nu_{\rm eff}$ than with the average density, whose increase was already observed to decrease the density peaking [10,11].

In order to explore the physics of the dependence of density peaking on collisionality we have considered two theoretical transport models, the Weiland model [12] and the GLF23 model [13], regularly applied for heat transport modeling of tokamak plasmas. These two models were chosen because they adopt complementary approaches, although they are both based on the fluid description of ITG and TEMs. The Weiland model is a reactive collisionless drift-fluid model, whereas the GLF23 model is a gyro-Landau-fluid model including the effects of collisions and resistivity on the electrons, as well as a fluid closure involving dissipative terms (although a collisional extension of the Weiland model has been proposed, we do not consider it here, in agreement with the application of this model by Weiland and co-workers [14]). Both the models provide expressions for heat and particle fluxes by means of quasilinear formulations. Transport simulations with the two models have been performed over a representative set of 30 plasmas of the database included in Fig. 1(a), covering the interval $0.1 \leq \nu_{\rm eff} \leq 2$. Plasma parameters are plasma current $I_p = 1$ MA, vacuum magnetic field B_t between 2.0 and 2.6 T, low triangularity $\delta < 0.2$, $P_{NBI} \simeq 5$ MW, $q_{95} \simeq 4$, whereas the average volume electron density $\langle n_e \rangle_{\rm Vol}$ varies between 2.9 to 8.6×10^{19} m^{-3} and the effective charge number is around 2.5 for low density plasmas and below 2 for high density plasmas. Simulations are performed in a predictive way, with an ASTRA transport code, by computing the plasma density, the electron, and the ion temperature, as well as the plasma current profiles, and thereby treating heat and particle transport, as well as the poloidal magnetic field diffusion consistently. Neoclassical effects are included, and the plasma conductivity is assumed neoclassical. Results of both the models are insensitive to arbitrary variations of the particle source profile and the predicted density peaking must be regarded as independent of the shape of the particle source profile. Further details about the transport modeling are provided in an extended article [15]. The results of the transport simulations are plotted in Fig. 2. Here the usual dimensionless parameters used in drift wave theory are used to plot both the experimental measurements and the simulation results: $\eta_\sigma = L_{n\sigma}/L_{T\sigma}$, $\epsilon_{n\sigma} = 2L_{n\sigma}/L_B$ (where $1/L_{n\sigma} = -d\ln n_\sigma/d\rho$, $1/L_{T\sigma} = -d\ln T_\sigma/d\rho$, $1/L_B = |d\ln B/d\rho| \simeq 1/R$ are the inverse gradient lengths, σ stands for species indexes i and e, and B is the total magnetic field). Radial derivatives are computed with respect to the flux label $\rho \doteq \rho_\phi a$, for both experimental and simulated profiles ($\rho_\phi \doteq \sqrt{\Phi/\Phi_{\rm edge}}$, where Φ is the toroidal magnetic flux, and a is the minor radius at the outer midplane). In Fig. 2(a) ϵ_{ne}, computed as the average value between $\rho_\phi = 0.4$ and $\rho_\phi = 0.7$, is plotted as a function of the volume average plasma density. The experimental points (stars) show that the density gradient length increases with increasing density, and this reflects the collisionality dependence shown in Fig. 1(a). Such a behavior is not predicted by the transport simulations performed with the reactive collisionless model (full squares), which yields a density gradient length independent of the plasma density. As also shown by Figs. 2(b) and 2(c), the 30 simulations with this model provide always the same results in these dimensionless plots. On the contrary, the dissipative collisional model, GLF23 (open circles), predicts density gradient lengths in good agreement with the experimental measurements. This indicates that the observed variation of density peaking can be ascribed to the effect of collisionality, in agreement with the experimental results. In order to verify such a conjecture we have modified the GLF23 model in a reactive gyro-Landau-fluid (RGLF) model, by neglecting collisionality and resistivity, and by closing the fluid equations with the same basic assumption of

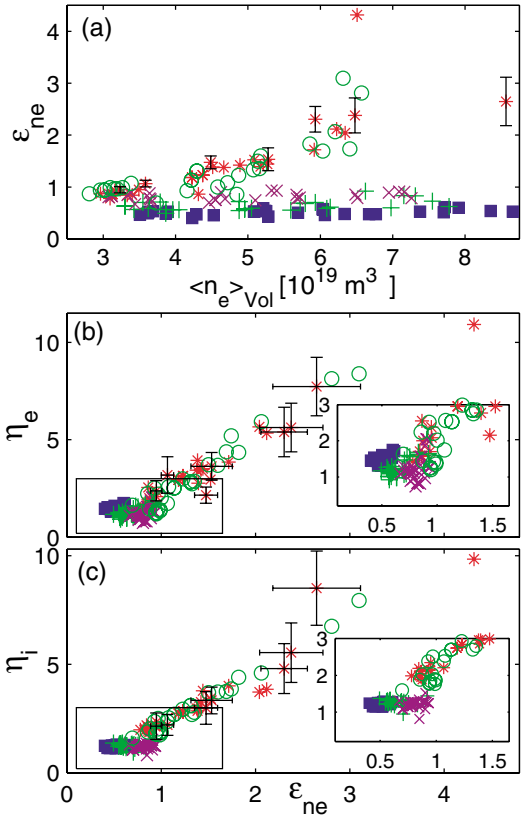

FIG. 2 (color online). Results of transport simulations with four different models, plotted in dimensionless parameters ϵ_{ne} , η_e , η_i : experimental data (stars), Weiland model (full squares), GLF23 (open circles), RGLF (+), collisionless GLF23 (×). Small panels show a zoom of the plot enclosed in the respective box.

the Weiland model, namely, that the first order perturbation of the distribution function is a perturbed Maxwellian. The RGLF model yields predictions which are remarkably close to those of the Weiland model, when presented in the dimensionless plots of Fig. 2 ("+" symbols). Values of ϵ_{ne} independent of the average plasma density are found, indicating that such a behavior is a general prediction of all reactive collisionless drift wave models. We have also performed a fourth set of simulations with a dissipative but collisionless model, obtained directly by switching off collisions in the GLF23 model. The results of these simulations ("×" symbols) still show the independence of ϵ_{ne} on the volume average density and assess the validity of our conjecture: the experimentally observed drop of density peaking can be explained by the effects of collisionality on drift wave (ITG and TEM) instabilities. We mention that the GLF23 model simulations give satisfactory results with respect to usual figures of merit [15].

We recall that quasilinear fluid models on drift wave instabilities predict a full transport matrix for heat and particle fluxes [16]. Fluxes are driven not only by diagonal terms (i.e., a density gradient for a particle flux), but also by off-diagonal terms (i.e., temperature gradients) and pinch terms. The Weiland model provides analytical expressions for heat and particle fluxes in terms of local plasma parameters, and this can be considered as an instructive collisionless limit. It is found that the contribution to the particle flux provided by the electron temperature gradient (thermodiffusion) is directed inwards for usual monotonic temperature profiles, for plasmas dominated by the ITG instability, as those analyzed in the present work. When the frequency of the most unstable mode is in the electron drift direction (TEM dominated plasma), the thermodiffusive flux can change sign and be directed outwards. Instead, the contribution given by the particle pinch is always directed inwards, for any value of the mode frequency. This term, which is usually dominant compared to the thermodiffusive flux, must be ascribed to the presence of a radially dependent magnetic field, due to the toroidal geometrical structure of the tokamak, and arises from the curvature drift. A recent more general analysis [17] has shown that when ITG modes dominate this contribution turns out to be proportional to the magnetic shear and describes the same physics of models based on turbulent equipartition [18].

The analytical procedure applied to the reactive collisionless Weiland model is not applicable in practice to the more complex dissipative collisional model (GLF23). This limitation is overcome, and a physical insight on the effect of collisionality on the different diagonal, off-diagonal, and pinch contributions to the total particle flux is obtained, by defining incremental diffusivities in terms of the three physics variables which are the unknowns of the coupled set of transport equations, namely, n_i, T_e, and T_i,

$$\tilde{D}_{nn} \doteq \frac{-\partial q_n}{\partial(\partial \ln n_i/\partial\rho)}, \qquad \tilde{D}_{n\sigma} \doteq \frac{-\partial q_n}{\partial(\partial \ln T_\sigma/\partial\rho)}, \tag{1a}$$

where σ stands for species indexes e, i, and q_n is defined as total particle flux per particle, with the dimensions of a speed. The pinch contribution is then evaluated as

$$\tilde{v}_n \doteq q_n + \tilde{D}_{nn}\frac{1}{n_i}\frac{\partial n_i}{\partial\rho} + \tilde{D}_{ne}\frac{1}{T_e}\frac{\partial T_e}{\partial\rho} + \tilde{D}_{ni}\frac{1}{T_i}\frac{\partial T_i}{\partial\rho}. \tag{1b}$$

The numerical computation of the transport coefficients defined in Eqs. (1a) and (1b) have been performed with the GLF23 model considering as input the experimental plasma profiles of the database previously used for the transport simulations. The particle fluxes per particle $-\tilde{D}_{nn}\partial \log n_i/\partial\rho$, $-\tilde{D}_{ne}\partial \log T_e/\partial\rho$, $-\tilde{D}_{ni}\partial \log T_i/\partial\rho$, and $\tilde{v}_n$ are plotted as functions of $\nu_{\rm eff}$ in Fig. 3, considering average values between $\rho_\phi = 0.4$ and $\rho_\phi = 0.7$. Consistently with the Weiland model, the diagonal flux $-\tilde{D}_{nn}\partial \log n_i/\partial\rho$ is directed outwards, whereas the flux driven by the electron temperature gradient $-\tilde{D}_{ne}\partial \log T_e/\partial\rho$, as well as the anomalous pinch $\tilde{v}_n$, is directed inwards (negative values in Fig. 3). All the terms are large at low collisionality and decrease with increasing collisionality, taking relatively low values for $\nu_{\rm eff} \geq 1$. The net particle flux must be interpreted as the result of the balance among inward and outward, diagonal and out-of-diagonal (off-diagonal and pinch) fluxes. Such a balance of fluxes determines the shape of the density profiles, that is, the density peaking. This explains why both the GLF23 and Weiland models show a strong insensitivity of the predicted density profile on the detailed shape of the particle source profile. Indeed the net flux, which at steady state is equal to the volume integral of the particle source, is smaller than each of the diagonal and out-of-diagonal contributions, and particularly it becomes negligible in the low collisionality regime $\nu_{\rm eff} \ll 1$. The effect of collisionality on density peaking can be investigated now by introducing an effective total anomalous pinch $\tilde{V}$, which includes all out-of-diagonal contributions defined in Eqs. (1a) and (1b),

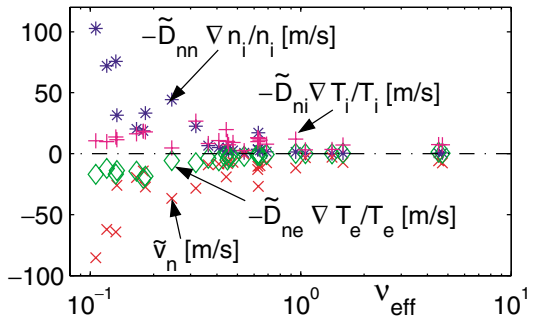

FIG. 3 (color online). Diagonal and out-of-diagonal particle flux contributions predicted by GLF23 and defined by incremental diffusivities [Eqs. (1a) and (1b)], versus the effective collisionality $\nu_{\rm eff}$.

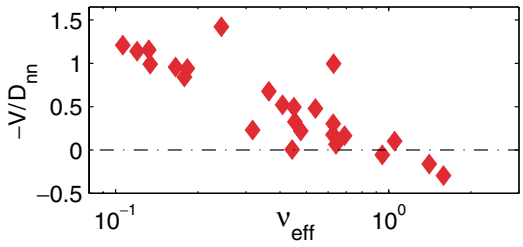

FIG. 4 (color online). Ratio of the effective total pinch to the diagonal diffusivity [Eq. (2)] versus ν_{eff}.

$$\tilde{V} \doteq q_n + \tilde{D}_{nn}\frac{1}{n_i}\frac{\partial n_i}{\partial \rho} = -\tilde{D}_{ne}\frac{1}{T_e}\frac{\partial T_e}{\partial \rho} - \tilde{D}_{ni}\frac{1}{T_i}\frac{\partial T_i}{\partial \rho} + \tilde{v}_n.$$

Therefore,

$$-\frac{\tilde{V}}{\tilde{D}_{nn}} = -\frac{q_n}{\tilde{D}_{nn}} - \frac{1}{n_i}\frac{\partial n_i}{\partial \rho} \sim -\frac{1}{n_i}\frac{\partial n_i}{\partial \rho}, \qquad (2)$$

that is, the ratio $-\tilde{V}/\tilde{D}_{nn}$ provides an estimate on how the transport model reacts at the variation of a given parameter to lead to density peaking. Figure 4 illustrates that $-\tilde{V}/\tilde{D}_{nn}$ decreases with increasing collisionality (ν_{eff}), and so does the predicted density peaking [Fig. 2(a)]. Although both inward and outward fluxes decrease with increasing collisionality, inward fluxes decrease more, and this explains the observed flattening of the density profiles with collisionality. At high collisionality $-\tilde{V}/\tilde{D}_{nn}$ changes sign, suggesting that, without neoclassical effects, the predicted profile, with a given boundary condition, could become hollow. Transport simulations at high collisionality ($\nu_{\mathrm{eff}} \simeq 1$), with the GLF23 transport model alone, neglecting the Ware pinch, show that density profiles are flat, and that the observed peaking is mainly determined by neoclassical effects, which are instead negligible at low collisionality (Fig. 5). This explains why anomalous particle pinch effects are not detected in experiments with plasmas at very high collisionality, that is, close to the density limit in present large tokamak experiments such as AUG [7] and JET [8]. Otherwise, in lower collisionality plasmas, anomalous pinch effects are correctly invoked to explain the experimental density peaking in tokamaks [2–6].

In conclusion, for the first time clear experimental evidence has been provided that density peaking in a tokamak plasma is connected with the collisional regime. The density peaking drops with increasing collisionality, and such dependence is well described by a dimensionless collisional frequency ν_{eff} defined as the ratio of the electron-ion collision frequency to the curvature drift frequency. The relation between density peaking and collisionality can be explained by quasilinear fluid drift wave models, provided that they include the effects of collisional processes on the electrons. Anomalous particle pinch effects are dominant at low collisionality, while they strongly decrease when ν_{eff} approaches unity. The neoclassical Ware pinch plays an essential role only in high collisionality plasmas. These theoretical results reconcile apparently contradictory recent experimental observations, some indicating the existence of an anomalous particle pinch [2–6], others denying its existence [7,8]. The present results point out that a different particle transport must be expected in burning plasmas with respect to the one observed in present experiments with plasma densities at the same large fraction of the limit plasma density, since in a burning plasma ν_{eff} is expected to be almost 2 orders of magnitude smaller.

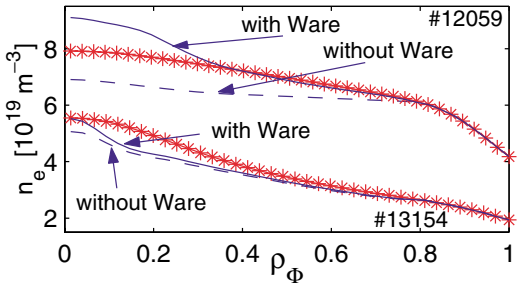

FIG. 5 (color online). Two representative simulations, with the GLF23 model, at low ($\nu_{\mathrm{eff}} \simeq 0.1$) and high ($\nu_{\mathrm{eff}} \simeq 1$) collisionality, with (solid line) and without (dashed line) the inclusion of the neoclassical Ware pinch. Experimental profiles are plotted with stars.

The authors thank X. Garbet and J. Stober for valuable and stimulating discussions, as well as J. Kinsey, R. E. Waltz, and J. Weiland for providing subroutines relative to the transport models. One of the authors (C.A.) acknowledges financial support for this work from the EURATOM programme of the European Community in the form of a Marie Curie Individual Fellowship, Contract No. FU05-CT-2002-50502.

[1] A. A. Ware, Phys. Rev. Lett. **25**, 916 (1970).
[2] D. R. Baker *et al.*, Nucl. Fusion **40**, 1003 (2000).
[3] M. Z. Tokar *et al.*, Phys. Rev. Lett. **84**, 895 (2000).
[4] H. Weisen and E. Minardi, Europhys. Lett. **56**, 542 (2001).
[5] G. T. Hoang *et al.*, Phys. Rev. Lett. **90**, 155002 (2003).
[6] L. Garzotti*et al.* (to be published).
[7] J. Stober *et al.*, Nucl. Fusion **41**, 1535 (2001).
[8] M. Valovic *et al.*, Plasma Phys. Controlled Fusion **44**, 1911 (2002).
[9] G. Tardini *et al.*, Nucl. Fusion **42**, 258 (2002).
[10] A. G. Peeters *et al.*, Nucl. Fusion **42**, 1376 (2002).
[11] K. Borrass *et al.*, Nucl. Fusion **42**, 1251 (2002).
[12] J. Weiland, A. Jarmén, and H. Nordman, Nucl. Fusion **29**, 1810 (1989).
[13] R. E. Waltz *et al.*, Phys. Plasmas **4**, 2482 (1997).
[14] P. Strand *et al.*, Nucl. Fusion **38**, 545 (1998).
[15] C. Angioni *et al.*, Phys. Plasmas (to be published).
[16] H. Nordman *et al.*, Nucl. Fusion **30**, 983 (1990).
[17] X. Garbet *et al.* (to be published).
[18] D. R. Baker and M. N. Rosenbluth, Phys. Plasmas **5**, 2936 (1998).